U.S. DEPARTMENT OF ENERGY | Office of Science

DOE/SC-CM-25-001

FY 2025 First Quarter Performance Metric: Demonstrating Use of E3SM with an Urban Canopy Parameterization for Modeling Urban Impact on Local-to-Regional Heat Extremes

TC Chakraborty
Jianfeng Li
Lingcheng Li
Gautam Bisht
L Ruby Leung
Ian Kraucunas

January 2025

DISCLAIMER

Contents

Figures

Tables

1.0 Product Definition

Urban areas exhibit distinct biophysical, morphological, and thermodynamic characteristics that influence local and regional weather and climate. These impacts include changes to the surface energy budget, near-surface meteorology, atmospheric composition, hydrological cycle, energy systems, and carbon cycle (Arnfield 2003, Qian et al. 2022). Urbanization disproportionately affects local populations by altering weather, particularly heat extremes (Tuholske et al. 2021). However, limited observations and model deficiencies hinder the understanding of urban systems (Grimmond 2011, Muller et al. 2013). Despite advancements, key aspects of urbanization, such as spatial variability and temporal evolution, remain poorly captured in models, especially Earth system models (ESMs), which are essential for studying climate processes (Chakraborty and Qian 2024). As we move from rural to suburban to urban regions, we expect sharp gradients in temperature, humidity, wind, and cloud cover that ESMs at coarse resolutions cannot resolve. The challenges of accurately representing within-city variability, relevant for examining community-scale heat hazards, highlight the need for improving ESM modeling capabilities to address uncertainties in urban environments (Sharma et al. 2021).

Most ESMs have limited or no representation of urban areas due to a legacy focus on large-scale climate impacts and coarse model grids that overlook urban processes (Zheng et al. 2021). The U.S. Department of Energy's (DOE) Energy Exascale Earth System Model (E3SM; Golaz et al. 2019) is one of the few exceptions, incorporating an urban canopy model from the Community Land Model (CLM) using an "urban canyon" approach (Oleson et al. 2010) that represents roofs, walls, and canyon floors (Figure 1a). A global urban surface biophysical data set (Jackson et al. 2010), critical for constraining the surface energy budget, is also embedded in the E3SM Land Model (ELM). However, this model has two major limitations.

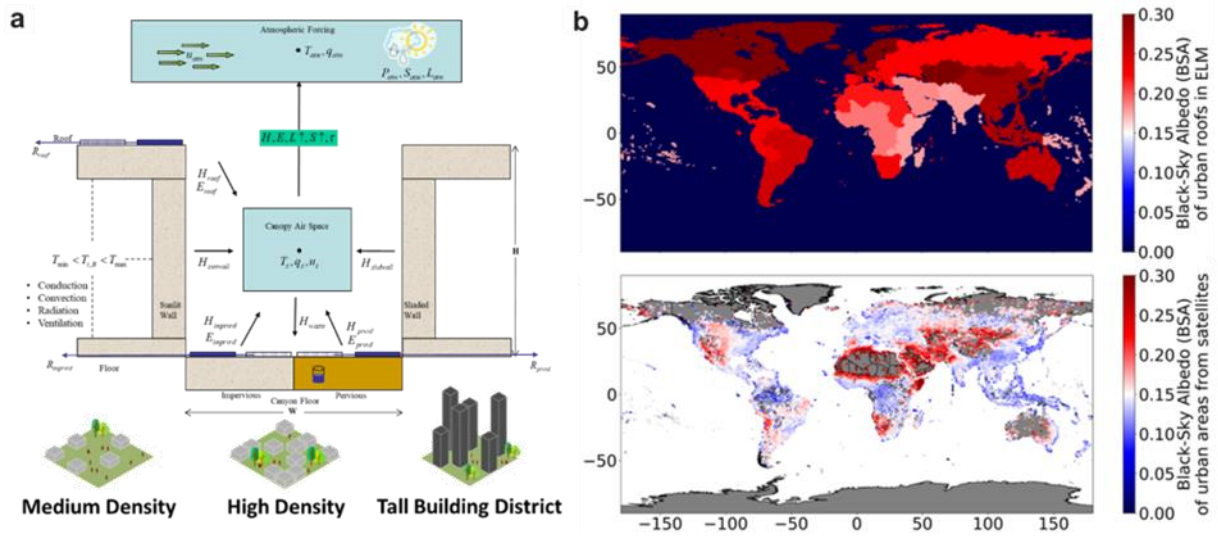

Figure 1. Panel a shows a schematic of the urban canopy structure within the E3SM Land Model (modified from Ching, 2013). Panel b shows the global spatial distribution of black-sky albedo of urban roofs, as prescribed in the current urban module of E3SM (top), and a similar variable (black-sky albedo of urban land) estimated from Moderate Resolution Imaging Spectroradiometer (MODIS) satellite imagery (bottom).

First, the urban surface data set in ELM is coarse-grained and outdated. Urban areas are categorized into three density classes across 33 global regions, with uniform radiative, morphological, and thermal properties that fail to capture real-world variability. For example, the prescribed albedo values differ significantly from satellite observations, which reveal greater variability within and across these 33 regions (Figure 1b). Poorly constrained urban parameters have a larger impact on model performance than model complexity, as evidenced by discrepancies in urban heat island (UHI) intensity simulations (Chakraborty et al. 2021, Grimmond 2011). Second, it neglects a key feature of many urban areas by not considering any vegetation within the urban canyon. As such, urban areas are treated as biologically inactive, with pervious surfaces modeled as bare soil. This neglects the critical role of urban vegetation in influencing temperature, air quality, and the water, energy, and carbon cycles within cities (Paschalis et al. 2021). In the context of extreme heat, it is well established that urban greenery mitigates daytime heat hazards (Ziter et al. 2019), a key requirement for effective climate adaptation in a warming world. While meso- and micro-scale models have advanced to include urban vegetation explicitly (Krayenhoff 2021), ESMs have lagged, often relying on outdated tiled approaches that cannot resolve spatial variability within urban areas (Krayenhoff 2020).

With ESMs now running at finer spatial resolutions, these deficiencies become more critical. For example, even when the Simple Cloud Resolving E3SM Atmosphere Model (SCREAM; Caldwell 2021) is run at km scale, the land cover constraints are still coarse, thus underestimating near-surface heterogeneity. High-resolution modeling, in theory, can reveal urban heat hotspots, UHI patterns, and urban-induced cloud formation (Theeuwes et al. 2019), aiding urban planning, isolating communities vulnerable to urban environmental stressors (Chakraborty et al. 2023), and guiding stormwater management strategies. However, SCREAM would still underestimate variability within and across cities due to its simplified representation of urban areas. To accurately capture urban climate signals, models must incorporate spatially continuous and biologically active urban representations, particularly for fine-scale simulations. This would improve insights into urban impacts and enhance planning for climate adaptation and resilience.

This report documents recent improvements in ELM and the ELM urban model through the Integrated Coastal Modeling (ICoM) project and a DOE Early Career project that advance surface constraints for high-resolution urban-resolving E3SM simulations. We explore these improvements and their implications for urban heat and heat stress using both land-atmosphere coupled SCREAM simulations at 3.2 km and ELM land-only simulations over the United States for a heatwave period in July 2020. The coupled simulations run with and without spatially explicit urban surface data sets show improvements in capturing urban heat signals and their spatial and diurnal variability, while the land-only simulations allow us to estimate the sensitivity of urban heat to radiative and morphological urban parameters.

2.0 Product Documentation

This report documents the modeling of urban heat extremes in the contiguous United States using SCREAM with regional refinement capability. To accommodate km-scale modeling, we update the surface data of SCREAM based on several 1-km data sets to resolve spatial variability more realistically.

2.1 High-Resolution Land Cover Constraints

A global 1-km data set of land surface parameters was developed by Li et al. (2024) as part of the ICoM project using a combination of data sources. This data set, covering the years 2001 to 2020, provides higher-resolution information and more spatial variability of land use and land cover (LULC), vegetation properties, soil properties, and topography than conventional coarse-resolution data sets. Specifically, we update organic matter, clay, and sand percentages in soil, lake, and glacier percentages, the fractions of different plant function types in natural vegetation, leaf area index, stem area index, and canopy height information in the SCREAM surface data.

2.2 Global Spatially Explicit Urban Biophysical Properties for Urban-Scale Modeling

The urban component of E3SM requires facet-level (roofs, walls, roads, etc.) properties critical for constraining the surface energy budget and anthropogenic signals. Recent work supported by a DOE Early Career project has developed U-Surf, a new global data set of urban surface parameters at a 1-km resolution (Figure 2b). U-Surf leverages high-resolution satellite remote-sensing data, machine learning techniques, and planetary-scale geospatial analyses on cloud computing platforms to generate a comprehensive and internally consistent set of biophysical parameters for urban areas worldwide. These parameters include radiative, structural, and thermal properties, aligning with the structural requirements of various urban canopy models, particularly E3SM (Figure 2). This compatibility enables realistic comparisons of urban climate signals both within and across cities. More details can be found in Cheng et al. 2024.

We update urban properties in the SCREAM surface data using U-Surf except for urban fractions, which are from another global 1-km data set of annual urban dynamics between 1870 and 2100 developed by Li et al. (2021), who trained an urban cellular automata model using satellite observations of urban extent between 1992 and 2013 and ran the model to simulate urban dynamics before 1990 and after 2020 under five Shared Socioeconomic Pathways (SSPs). The data set thus provides temporally continuous self-consistent high-resolution urban coverages, which is helpful in studies relevant to urban expansion and shrinkage. Urban fractions in 2010 from the data set are used to update our SCREAM surface data.

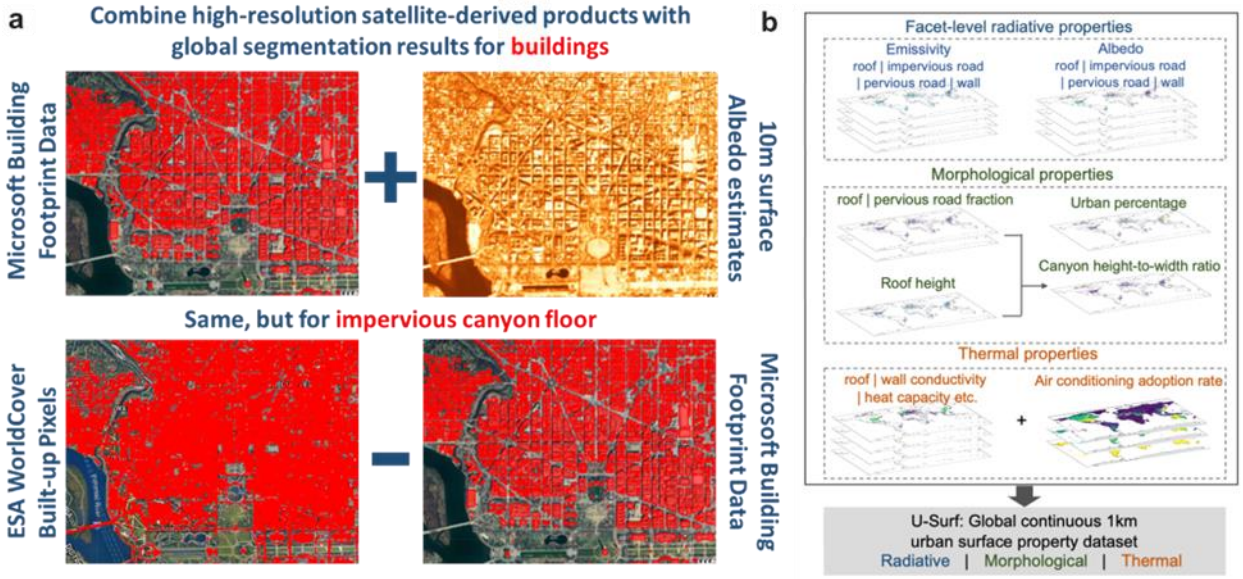

Figure 2. Panel a shows an example of how building footprint, high-resolution land cover, and high-resolution albedo estimates are combined to estimate roof and road albedo for incorporation into the model. Panel b gives an overview of all the urban facet-level radiative properties, morphological properties, and thermal properties that are included in the U-Surf data set.

2.3 Regionally Refined Simulations for Km-Scale Urban-Resolving Continental Simulations

Although the update of LULC percentages, soil properties, and vegetation parameters in the surface data can also influence the simulation of heat extremes, its comparison with the default ELM surface data set has already been performed by Li et al. (2024). In this report, we use this data set in all the simulations and focus on understanding how updated urban properties from U-Surf can alter the heat extreme simulation since these properties are more relevant to the urban model. We conduct two atmosphere-land coupled SCREAM simulations, one with the default urban properties (hereafter named the default simulation) and the other with U-Surf urban properties (hereafter named the U-Surf simulation) to investigate the potential impact of updated urban properties on the simulation of a heat wave that occurred in late July 2020 in the eastern United States. The simulation period is from July 18 to July 30 with the first day as spin-up. To reduce the computational cost, we run SCREAM on a regional refinement mesh (RRM) with a horizontal resolution of ~3.2 km over the contiguous U.S. (CONUS) and ~100 km for other areas globally (Figure 3a). The atmospheric initial condition is based on a combination of the hourly 3-km High-Resolution Rapid Refresh (HRRR) and 25-km ERA5 reanalysis data sets. The land's initial condition is obtained from a 10-year land-only simulation on the same SCREAM RRM constrained by atmospheric forcing in 2020 from ERA5. The SCREAM simulation uses prescribed hourly sea surface temperature (SST) from ERA5. Three-dimensional zonal and meridional winds, temperature, and specific humidity above 850 hPa are nudged towards hourly ERA5 reanalysis with a relaxation timescale of six hours for the coarse-resolution grids with equivalent physical grid spacing larger than 5 km. Finally, we regrid the coupled simulation outputs to 4 km to facilitate comparison and analysis.

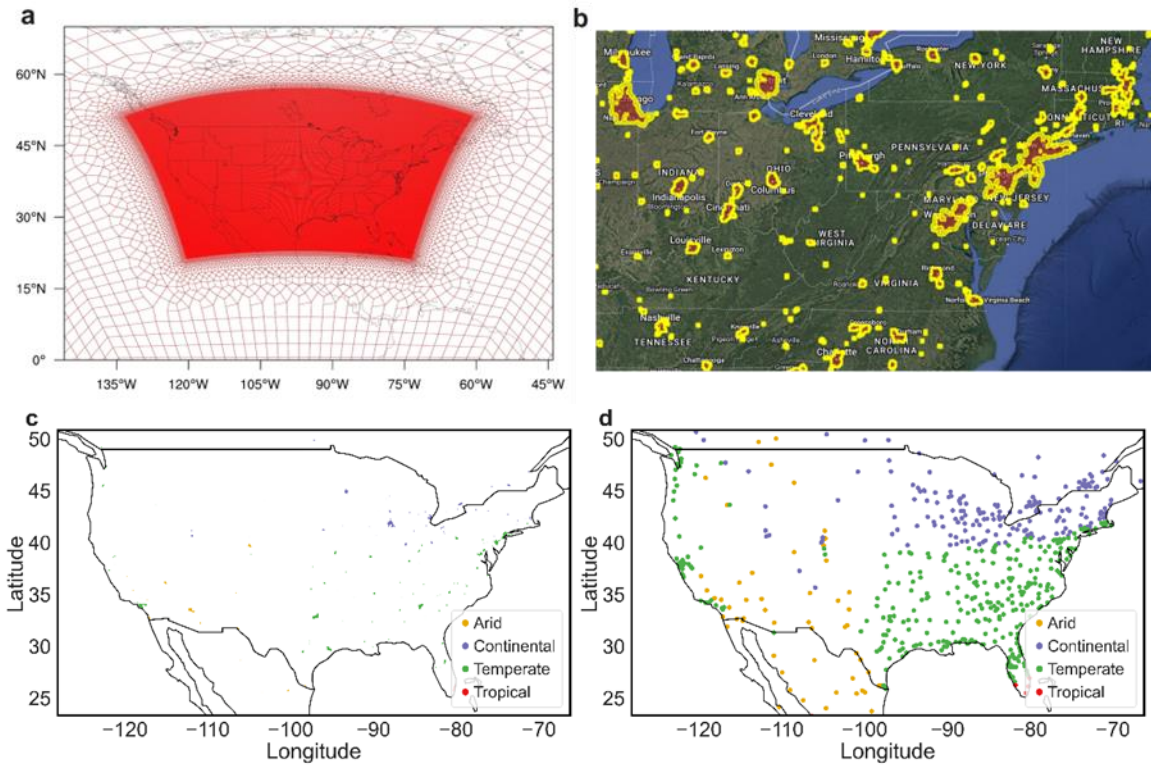

Figure 3. Panel a shows the regional refinement mesh over the continental U.S. used in our coupled and land-only simulations. Panel b shows the urban clusters and their equal-area surrounding rural buffers generated from the surface data set used in our SCREAM and ELM simulations. Panel c shows the location, extent, and background Köppen-Geiger climate zone of all 540 urban clusters. Panel d is similar to c, but shows the centroids of the clusters instead of their extent for improved visibility.

Besides the above two coupled simulations, we run five additional land-only simulations to resolve the distinct impacts of facet-level albedo, facet-level emissivity, and morphological (roof height, roof fraction, pervious road fraction, height of wind in canyon, and canyon height to width ratio) urban parameters from U-Surf on the heat extreme simulation (Table 1). The land-only simulation period is from July 19 to July 30, and the simulations are constrained by atmospheric forcing from the default coupled simulation. The restart file at 0:00Z on July 19 from the default coupled simulation is used as the initial condition for the land-only simulations except for the "All New Properties" simulation, which uses the restart file from the U-Surf coupled simulation due to different urban levels between the default and U-Surf urban property data set.

Table 1. Overview of the land-only offline simulations.

Simulation name	Default urban properties	U-Surf albedo parameters	U-Surf emissivity parameters	U-Surf morphological parameters	Other U-Surf urban properties
Default	Y				
Default + Albedo	Y	Y			
Default + Emissivity	Y		Y		
Default + Morphology	Y			Y	
ALL New Properties		Y	Y	Y	Y

In coarse-grid E3SM simulations, the urban climate signals are often calculated as the difference in simulated values for the urban and rural subgrids within each coarse model grid. However, this method cannot resolve individual urban areas, since a single ~1-degree grid includes multiple cities and even parts of other cities. Since we run these simulations at 3.2-km resolution, we can address this limitation. To delineate urban clusters, we vectorize the surface data set used in the simulations, with a threshold of 30% urban used to choose valid grids for analysis of urban effects. This threshold is consistent with the urban definition used in the MODIS land cover product. We generate 540 clusters within the model domain of the RRM using this method. We can then generate a region around each urban cluster, consistent with buffer-based methods used to estimate various urban climate signals. These rural references are created for each urban cluster and are roughly equal in area to the urban cluster they surround, using an iterative method on the Google Earth Engine platform (Gorelick et al. 2017) following Chakraborty et al. (2021).

3.0 Results

3.1 Evaluation of the Coupled Simulations against Weather Station Measurements

We first evaluate our coupled simulations against the Integrated Surface Database (ISD), which is a global database providing hourly surface observations from weather stations from numerous sources (Smith et al. 2011). Figure 4 shows the comparison of mean surface air temperature and relative humidity among the default and U-Surf coupled simulations and ISD during July 19-30, focusing on the results within the RRM of CONUS. Although SCREAM slightly overestimates air temperature while apparently underestimating relative humidity compared to ISD, both the default and U-Surf coupled simulations capture the air temperature and relative humidity spatial distributions well and identify extensive heat extremes in the central and eastern United States, especially in the southern Great Plains and the eastern coastal areas. Using U-Surf urban properties in SCREAM does not improve the simulation of the “bulk” characteristics of air temperature and relative humidity. A possible reason is that U-Surf is most relevant

to urban grids and its influence may be most significant in local urban and nearby rural areas. Therefore, we focus only on the urban pixels and clusters in our following analysis.

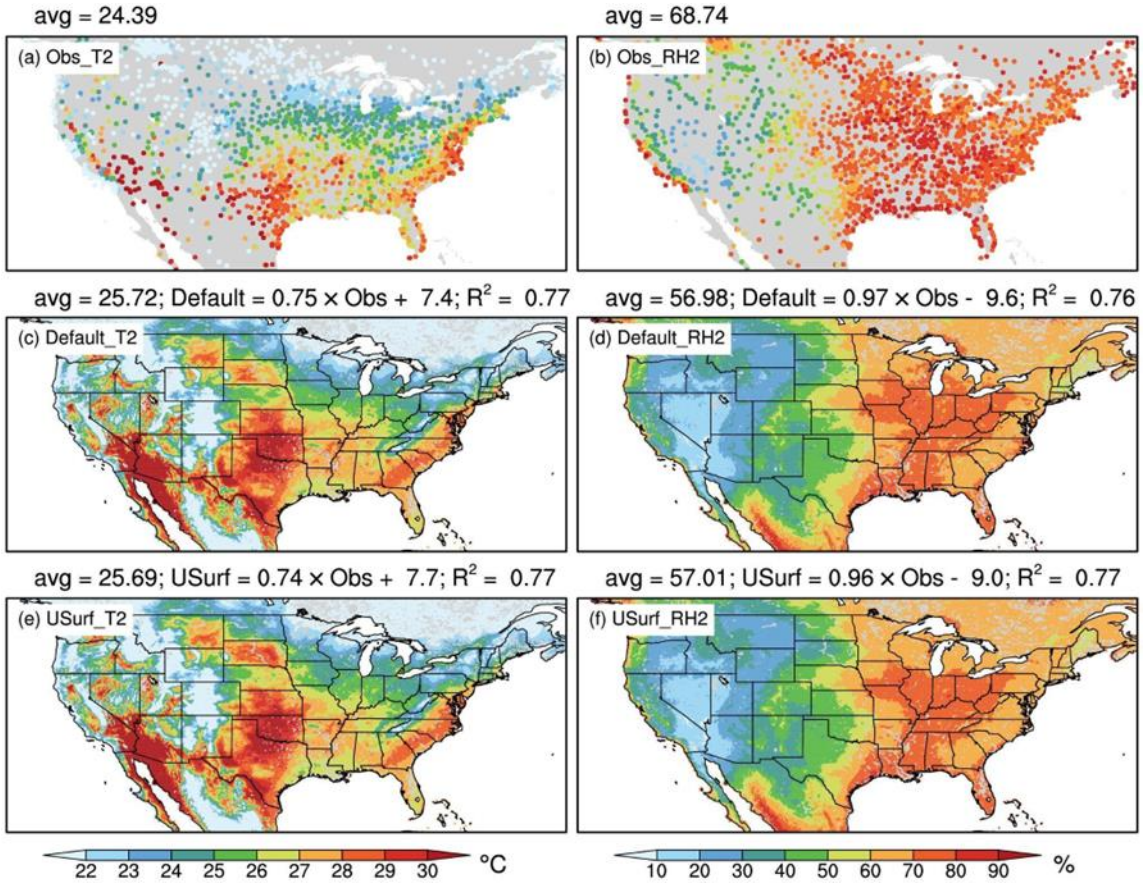

Figure 4. Comparison of mean air temperature (T2; panels a, c, e) and relative humidity (RH2; panels b, d, f) between the coupled simulations and the ISD observations. The first row is for ISD observations, and the second and third rows are for the default and USurf simulations, respectively. There are 2319 weather stations with T2 measurements and 2082 stations with valid RH2 observations (calculated from T2 and 2-m dew point temperature). The "avg" above each subplot indicates the corresponding average of all weather sites (or coincident grids for SCREAM simulations). The corresponding linear regression results between the coupled simulations and ISD observations are also shown above all panels.

3.2 Urban Heat Impacts from Coupled E3SM Simulations Using Updated Surface Constraints

From our coupled simulations, we examine mean surface climate variables, particularly air temperature and relative humidity, as well as their daytime and nighttime values. Here, daytime values are from all the time steps when the incoming shortwave radiation from the sun is greater than 0. Time steps with no incoming radiation are averaged to provide the nighttime values.

Capturing Spatial Variability of Urban Climate through Km-Scale Simulations

Our coupled simulations successfully capture the expected spatial distribution of temperature and relative humidity in and around cities (Oke 1979). Of note, urban areas tend to increase daytime air temperature locally, i.e., the UHI effect, with the impact dissipating as we move away from the urban core (Fig. 5a). In parallel, the relative humidity reduces locally over urban areas, sometimes also referred to as the urban dry island (UDI) effect (Wang et al. 2021). Since standard E3SM simulations are run at much coarser resolutions (~100 km), they would not be able to spatially disaggregate the variability of these signals over urban areas. Even SCREAM simulations with coarse-resolution land cover constraints cannot resolve urban areas and different degrees of urbanization.

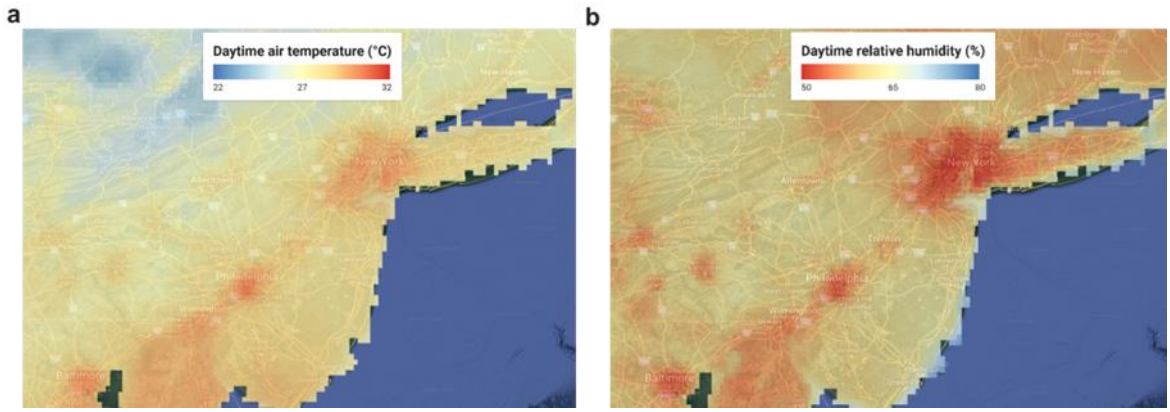

Figure 5. Daytime (a) air temperature and (b) relative humidity during the simulation period over part of the model domain in the eastern United States, intended to demonstrate the local-to-regional urban signals captured by the coupled simulations.

Improvements in Urban-Scale Temperature Simulations Using U-Surf

We compare our simulations with properties from U-Surf against the simulations using the default properties currently used in ELM. To do urban-relevant evaluations, we use a recently developed gridded air temperature data set as the reference (Zhang et al. 2022), because ground-based observations are rare within cities (see Section 3.1). The evaluations are then performed only for the urban clusters generated earlier, as well as their rural references so that the UHI can also be evaluated (Figure 6). Similar data sets are not available for humidity.

The spatial variability of temperature across urban clusters does not change much by using U-Surf. However, the bias and root mean square are both reduced. The mean bias error (MBE) is reduced from 0.68 °C to 0.43 °C. When we perform a similar evaluation over the rural buffers, we also find improvements in simulated mean air temperature, with MBE reducing from 0.47 °C to 0.33 °C. This improvement in the rural temperature is interesting because we only consider grids with no urban percentage within the rural buffers when estimating these signals. This suggests that the improvements in urban simulations due to U-Surf extend beyond, at least slightly, the boundaries of the urban area, potentially through horizontal advection in the atmosphere model (Debbage and Shepherd 2015).

Finally, we estimate the UHI as the difference between the temperatures in the urban clusters and their surrounding buffers. The MBE in the UHI is halved when U-Surf is used instead of the default

properties, highlighting the major benefit of using these updated high-resolution surface properties in urban-resolving simulations.

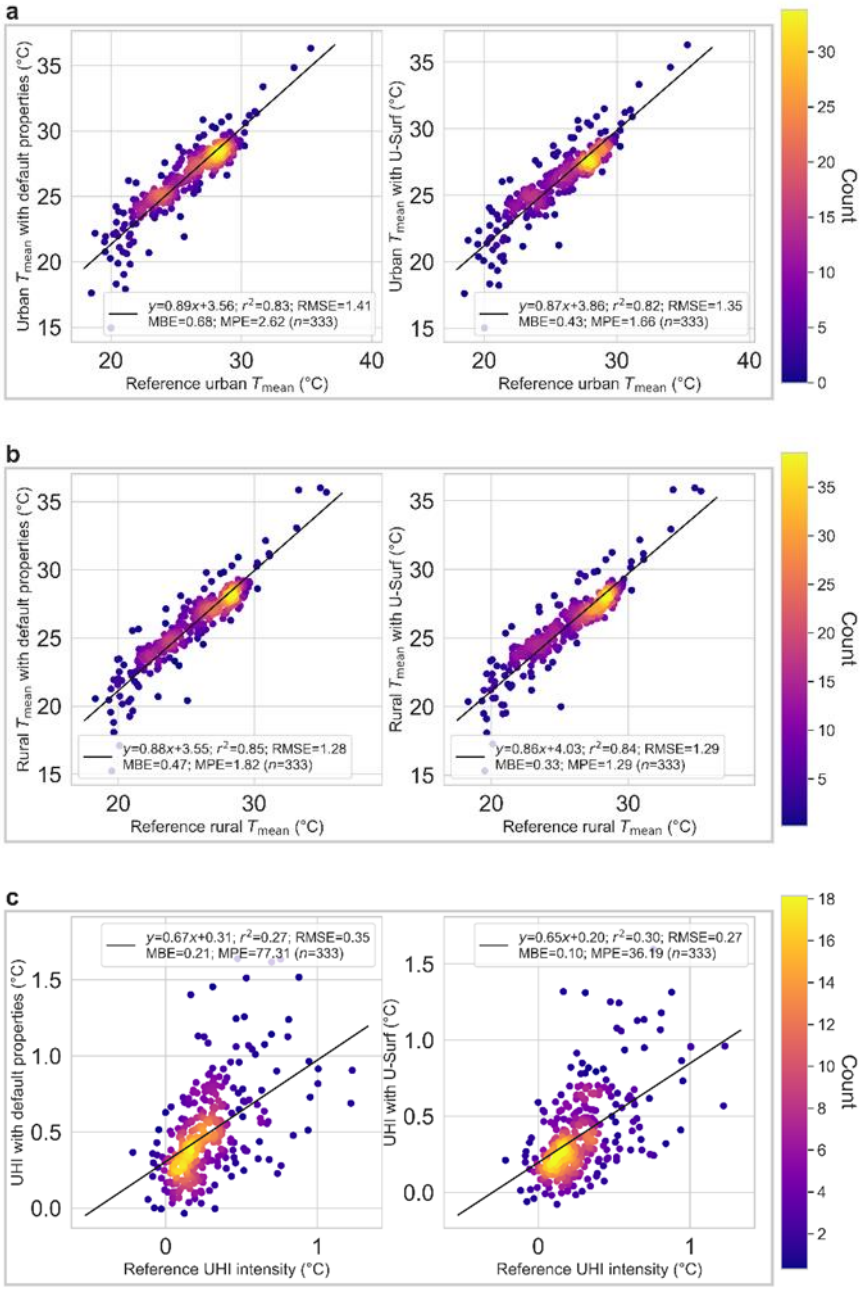

Figure 6. Comparison of the root-mean-square error (RMSE), MBE, and mean percentage error (MPE) of the simulated (a) urban temperature, (b) rural temperature, and (c) UHI intensity against a reference data set (Zhang et al. 2022) for the simulation period for the simulations with the default urban properties (left-hand plots) and the newly developed U-Surf data set (right-hand plots). Each dot corresponds to an urban cluster, with the density of urban clusters shown by the color. Linear regression lines are fitted to the results and shown in each panel.

3.3 Urban Temperature, Humidity, and Moist Heat across Regions

Cluster-Level Urban Heat, Dry, and Heat Stress Islands

Similar to the UHI, we calculate the UDI as the difference in relative humidity between the urban clusters and their rural references. We also calculate the heat index (Rothfusz 1990), used by the U.S. National Weather Service to indicate moist heat stress, from the air temperature and relative humidity estimates. The difference in heat index between the urban clusters and their rural references is then used to calculate the urban heat index island (UHII). The UHII matters more for local urban impact on heat hazard than UHI since it uses a physiologically relevant heat stress metric and is the result of the compensative effects of the UHI and the UDI (Chakraborty et al. 2022). Figure 7 shows the UHI, UDI, and UHII from the U-Surf coupled simulation for the entire simulation period and for daytime and nighttime. The results are as expected, with most urban clusters showing UHIs, UDIs, and UHIIs. The diurnal variability is also appropriately captured, with larger magnitudes of UHI, UDI, and UHII during nighttime (Figure 7g, 7h, 7i) compared to daytime (Figure 7d, 7e, 7f).

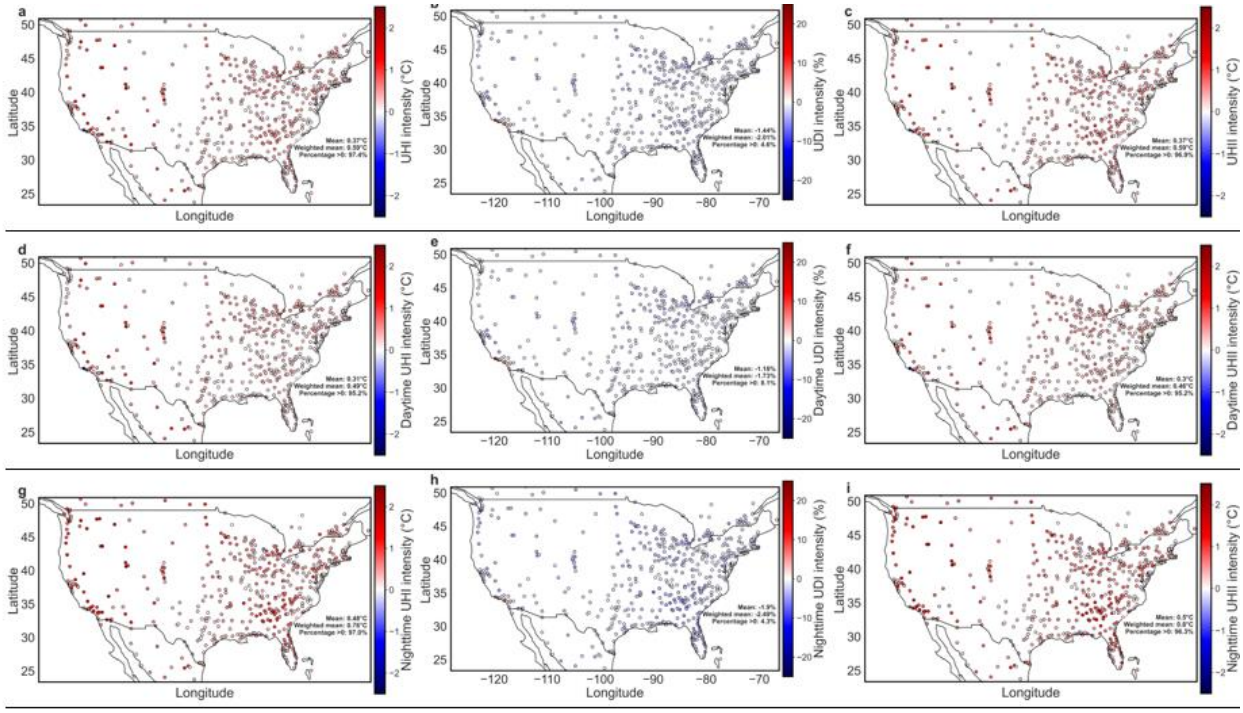

Figure 7. Simulated (a) UHI intensity, (b) UDI intensity, and (c) UHII for the generated urban clusters. Panels d, e, and f are the same as a, b, and c but for daytime values. Panels g, h, and i are for nighttime values. Each dot represents the spatial mean for an urban cluster. The urban spatial means, area-weighted spatial means, and percentage of urban clusters with values above 0 are also noted within each panel.

Variability across Climate Zones

An important theme in the UHI literature, and more recently the UDI literature, has been the dependence of the urban climate signals on background climate (Chakraborty and Lee 2019, Manoli et al. 2019, Zhao et al. 2014), especially the stronger urban signals in moist climates. When we separate the clusters into the Köppen-Geiger climate zones (Rubel and Kottek 2010), we find,

surprisingly, that the strongest UHI and UHII intensities are in the arid zone (Figure 8). One big reason why arid cities should have low UHI, and sometimes even appear as urban cool islands, is because arid cities can have more vegetation compared to the surrounding arid landscapes (Chakraborty and Lee 2019). However, the urban model in E3SM does not explicitly represent urban vegetation. Hence, this well-known urban climate signal in arid cities is not currently captured by E3SM and will require the development of urban vegetation in the land model, which is already underway.

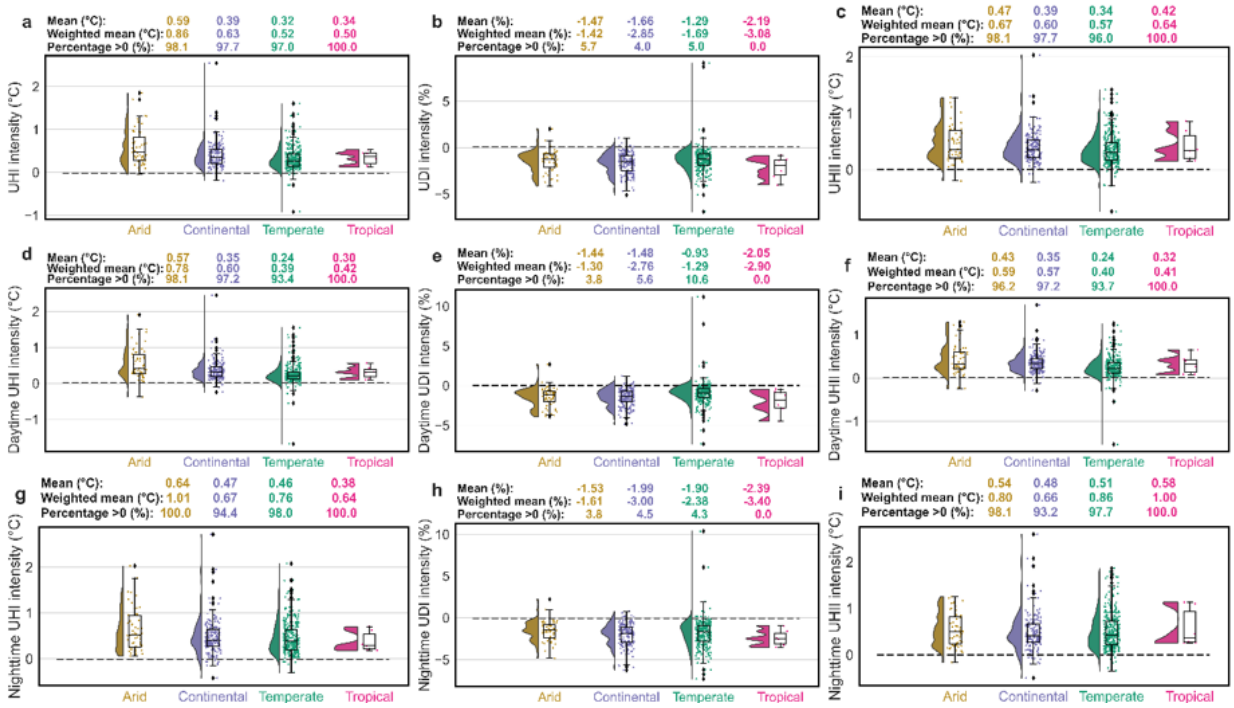

Figure 8. Distribution of (a) UHI intensity, (b) UDI intensity, and (c) UHII for every urban cluster in the RRM model domain by climate zone. The urban means, area-weighted means, and percentage of urban clusters with values above 0 are also noted for each case. Each dot represents the spatial mean for an urban cluster. The number of clusters in arid, continental, temperate, and tropical climates is 52, 177, 303, and 5, respectively. Panels d, e, and f are the same as a, b, and c but for daytime values. Panels g, h, and i are for nighttime values.

Comparing Buffer-Based and Subgrid-Difference Estimation of Urban Heat Signals

Since models often use subgrid differences or perturbation experiments (simulations with and without urban land) to estimate urban climate signals (e.g., Sarangi et al. 2021), while observational estimates often require buffer-based approaches (e.g., Yang et al. 2024), we take advantage of urban-resolving SCREAM simulations to compare both methods. These comparisons are done for daytime and nighttime UHI, UDI, and UHII (Figure 9). Although these variables estimated from both approaches show positive associations (slopes of the linear regression are greater than zero), the coefficients of determination (r2) are low to medium (generally below 0.40). In all cases, the buffer-based approach shows less variability in the urban climate signals than the subgrid-based approach. This makes conceptual sense since the rural buffer, even without any urban presence, would be significantly impacted by the urban area it surrounds (Yang et al. 2019). This means that the buffer-based approach, quite commonly used in the observational

and satellite remote-sensing literature, systematically underestimates the urban climate signals. This has broader implications for many of the global estimates of urban climate signals, including global UHI maps developed in the past (Clinton and Gong 2013, Yang et al. 2024), and suggests improving the estimation of UHI is an important application of km-scale simulations.

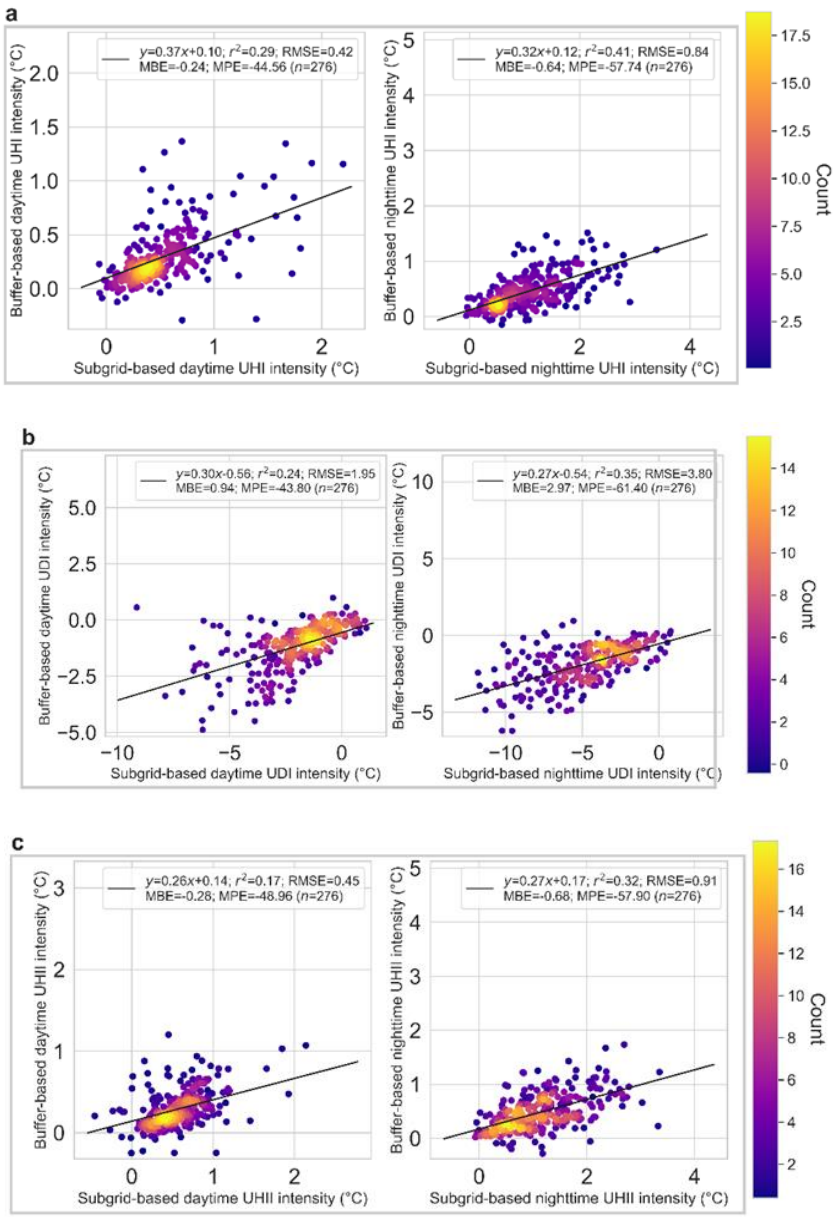

Figure 9. Comparison of the root mean square error (RMSE), mean bias error (MBE), and mean percentage error (MPE) of the simulated daytime (left-hand plots) and nighttime (right-hand plots) (a) UHI intensity, (b) UDI intensity, and (c) UHII intensity as calculated using the difference between urban and rural subgrid values in the model (subgrid-based approach) and the difference between urban values and their surrounding rural buffers (buffer-based approach). Each dot corresponds to an urban cluster, with the density of urban clusters shown by the color. Linear regression lines are fitted to the results and shown in each panel.

3.4 Sensitivity of Urban Heat to Urban Biophysical Properties in Land-Only Simulations

Impacts on Overall Distributions of Temperature

Analysis of averaged temperatures during the simulation period reveals distinct patterns in urban thermal characteristics arising from the use of different groups of surface properties from U-Surf versus the default data (Table 1). For urban air temperature distributions (Figure 10a), morphology and facet-level emissivity modifications cause significant reductions in mean urban temperatures, while facet-level albedo changes exhibit minimal impact. The reduction in urban temperatures due to the inclusion of U-Surf emissivity is expected since prescribed urban emissivity in models like ELM tends to be much lower than the emissivity estimated from satellite remote sensing. This would lead to high urban temperatures even if the outgoing longwave radiation is correctly simulated by the model (Chakraborty et al. 2021). For morphology, this may be due to the incorporation of finer-grain urban verticality in the surface data set, which can lead to additional convective cooling (Zhao et al. 2014). Rural temperature distributions (Figure 10b) show negligible sensitivity to urban properties, which makes sense since there is no advection in these land-only simulations. Future work will examine these same sensitivities using land-atmosphere coupled simulations to examine potential regional impacts of changes in urban biophysical properties. The change in the urban-rural temperature difference (UHI; Figure 10c) shows predominantly positive values, with morphological modifications producing the most substantial changes relative to the default configuration. The simulation incorporating all new properties shows the greatest reductions in UHI, primarily driven by the combined effects of morphology and emissivity modifications.

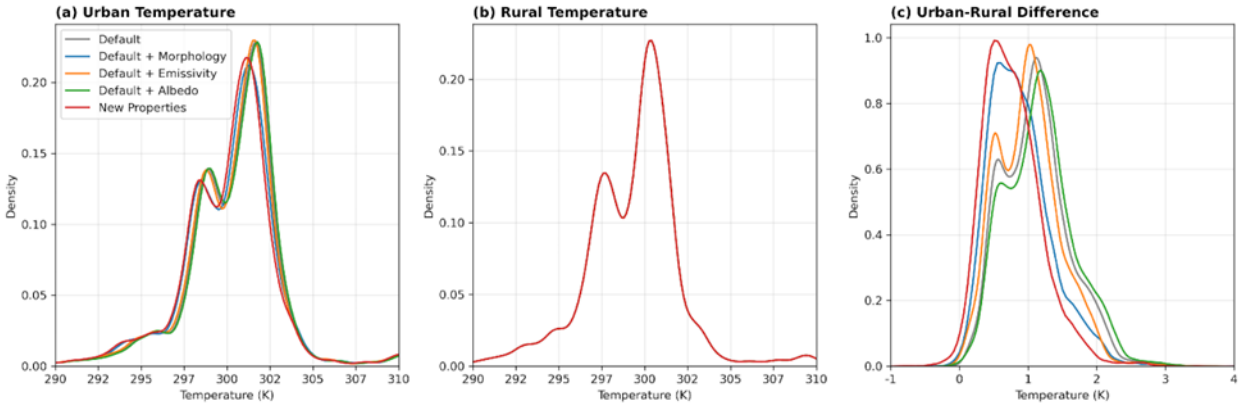

Figure 10. Kernel density estimate plots of averaged (a) urban air temperature, (b) rural air temperature, and (c) urban-rural temperature differences across the land-only simulations.

Impacts on Diurnal Variability of Temperature

The averaged diurnal cycle for the simulation period demonstrates that urban surface properties from U-Surf primarily influence the magnitude of temperature rather than its diurnal timing. Urban temperatures (Figure 11a) maintain consistent timing of peaks and troughs across simulations while exhibiting variations in magnitude based on property modifications. Rural temperatures (Figure 11b) show minimal inter-simulation variability throughout the averaged diurnal cycle. The UHI (Figure 11c)

displays a characteristic temporal pattern with minimum values during morning hours (approximately 8:00 AM local time) and maximum differences during nighttime periods. This is generally consistent with our existing understanding of the diurnality of UHIs and with the previous analysis on daytime and nighttime values (see Section 3.3). While the diurnal pattern persists across all simulations, the differences between them are not equal throughout the day, with stronger impacts of the urban properties seen during nighttime rather than during the early morning UHI minima.

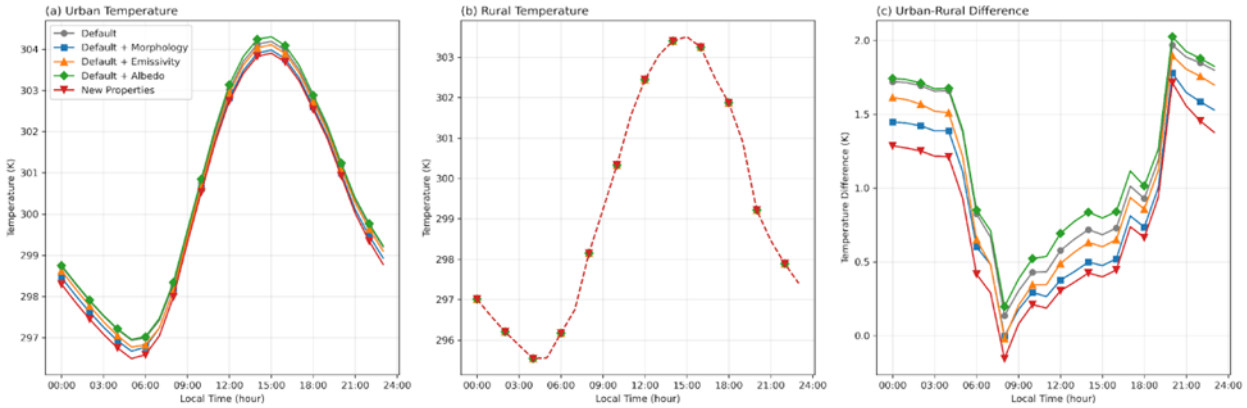

Figure 11. Mean diurnal cycles of (a) urban air temperature, (b) rural air temperature, and (c) urban-rural temperature differences averaged over the simulation period.

4.0 Summary and Future Work

In this report, we show the successful implementation of recent high-resolution surface data sets and urban facet-level properties to perform urban-resolving SCREAM-E3SM simulations. The newly developed surface constraints improve our ability to capture urban climate signals. However, the model still has issues when trying to capture the dependence of this urban climate signal on the background climate.

Future work includes the completion of ongoing work on developing the urban vegetation component within ELM, which is critical for capturing the urban warming signals across climate zones. This vegetation scheme would also require spatially continuous constraints for urban vegetation, which we are addressing through ongoing work to develop a global 1-km data set called U-Surf-Tree (Figure 12a). A lot of the ongoing development allowing urban-resolving simulations using E3SM would be critical for examining the impact of future urbanization. While we use only the Li et al. (2021) estimates of urban land in the simulations for this report, there are differences between urban extent across data sets (Figure 12b). As we incorporate future urbanization into E3SM, we plan to examine the impact of the choice of urban land projection data set (Figure 12c) on estimates of future climate. These future estimates of urban land, in conjunction with historical satellite imagery, will also be critical constraints for developing future estimates of biophysical urban properties for urban-resolving future climate modeling.

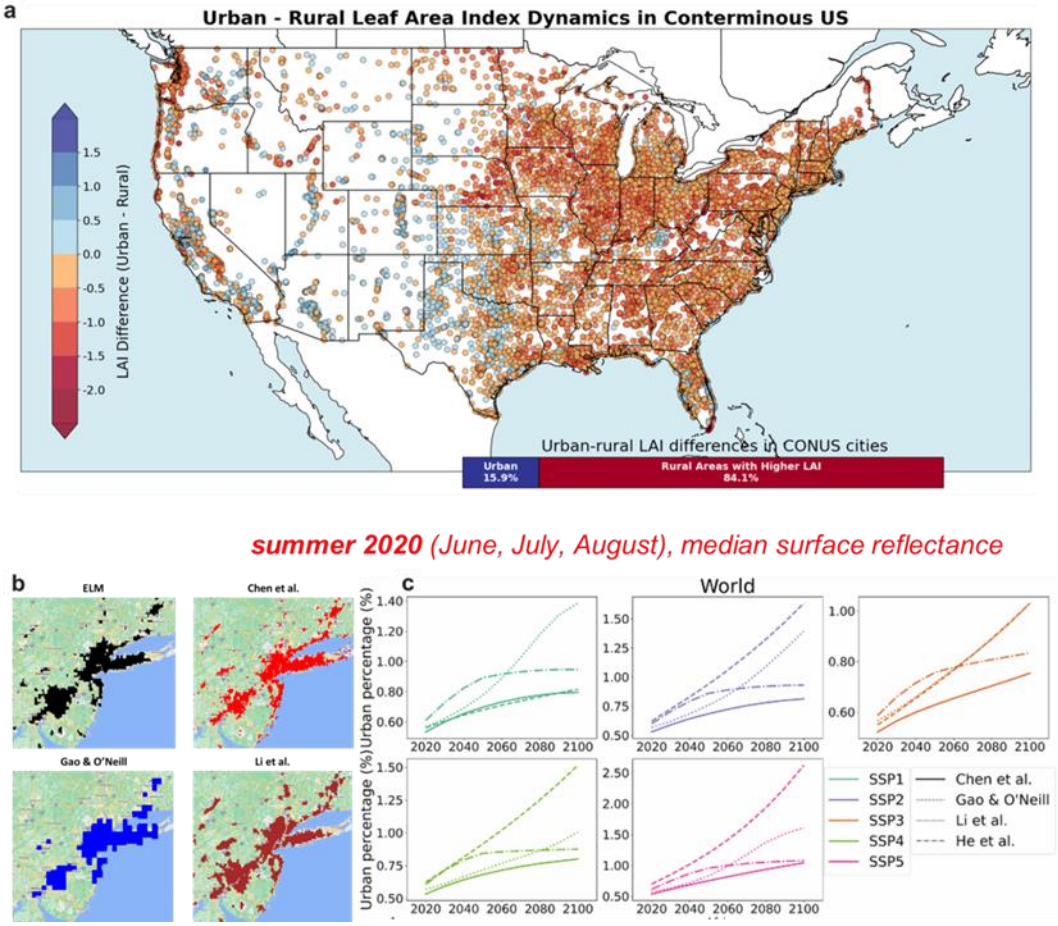

Figure 12. Panel (a) shows urban-rural difference in leaf area index (LAI) in the continental U.S. based on median satellite-derived surface reflectance values from ongoing work on developing a global data set of urban vegetation properties called U-Surf-Tree. Panel (b) shows the urban extent in the original E3SM land model and the 2020 estimate from three global urban projection products. Panel (c) shows a comparison of various urban projection data sets across SSPs till the end of the century.

5.0 References

Arnfield, AJ. 2003. "Two decades of urban climate research: A review of turbulence, exchanges of energy and water, and the urban heat island." *International Journal of Climatology* 23(1): 1–26, https://doi.org/10.1002/joc.859

Caldwell, PM, DR Terai, B Hillman, ND Keen, P Bogenschutz, W Lin, H Beydoun, M Taylor, L Bertagna, AM Bradley, TC Clevenger, AS Donahue, C Eldred, J Foucar, JC Golaz, O Guba, R Jacob, J Johnson, J Krishna, W Liu, K Pressel, AG Salinger, B Singh, A Steyer, P Ullrich, D Wu, X Yuan, J Shpund, H-Y Ma, and CS Zender. 2021. "Convection-Permitting Simulations with the E3SM Global Atmosphere Model." *Journal of Advances in Modeling Earth Systems* 13(11): e2021MS002544, https://doi.org/10.1029/2021MS002544

Chakraborty, T, and X Lee. 2019. "A simplified urban-extent algorithm to characterize surface urban heat islands on a global scale and examine vegetation control on their spatiotemporal variability." *International Journal of Applied Earth Observation and Geoinformation* 74: 269–280, https://doi.org/10.1016/j.jag.2018.09.015

Chakraborty, T, X Lee, S Ermida, and W Zhan. 2021. "On the land emissivity assumption and Landsat-derived surface urban heat islands: A global analysis." *Remote Sensing of Environment* 265: 112682, https://doi.org/10.1016/j.rse.2021.112682

Chakraborty, T, C Sarangi, and X Lee. 2021. "Reduction in human activity can enhance the urban heat island: Insights from the COVID-19 lockdown." *Environmental Research Letters* 16: 054060, https://doi.org/10.1088.1748-9326/abef8e

Chakraborty, T, ZS Venter, Y Qian, and X Lee. 2022. "Lower urban humidity moderates outdoor heat stress." *AGU Advances* 3(5): e2022AV000729, https://doi.org/10.1029/2022AV000729

Chakraborty, T. AJ Newman, Y Qian, A Hsu, and G Sheriff. 2023. "Residential segregation and outdoor urban moist heat stress disparities in the United States." *One Earth* 6(6) 738–750, https://doi.org/10.1016/j.oneear.2023.05.016

Chakraborty, T, and Y Qian. 2024. "Urbanization exacerbates continental- to regional-scale warming." *One Earth* 7(8): 1387–1401, https://doi.org/10.1016/j.oneear.2024.05.005

Cheng, Y, L Zhao, T Chakraborty, K Oleson, M Demuzere, X Liu, Y Che, W Liao, Y Zhou, and X Li. 2024. "U-Surf: A Global 1 km spatially continuous urban surface property dataset for kilometer-scale urban-resolving Earth system modeling." *Earth System Science Data*, https://doi.org/10.5194/essd-2024-416

Clinton, N, and P Gong. 2013. "MODIS detected surface urban heat islands and sinks: Global locations and controls." *Remote Sensing of Environment* 134: 294–304, https://doi.org/10.1016/j.rse.2013.03.008

Debbage, N, and JM Shepherd. 2015. "The urban heat island effect and city contiguity." *Computers, Environment and Urban Systems* 54: 181–194, https://doi.org/10.1016/j.compenvurbsys.2015.08.002

Golaz, J-C, PM Caldwell, LP Van Roekel, MR Petersen, Q Tang, JD Wolfe, G Abeshu, V Anantharaj, XS Asay-Davis, DC Bader, SA Baldwin, G Bisht, PA Bogenschutz, M Branstetter, MA Brunke, SR Brus, SM Burrows, PJ Cameron-Smith, AS Donahue, M Deakin, RC Easter, KJ Evans, Y Feng, M Flanner, JG Foucar, JG Fyke, BM Griffin, C Hannay, BE Harrop, MJ Hoffman, EC Hunke, RL Jacob, DW Jacobsen, N Jeffery, PW Jones, ND Keen, SA Klein, VE Larson, L Ruby Leung, H-Y Li, W Lin, WH Lipscomb, P-L Ma, S Marajan, ME Maltrud, A Mametjanov, JL McClean, RB McCoy, RB Neale, SF Price, Y Qian, PJ Rasch, JE Jack Reeves Eyre, WJ Riley, TD Ringler, AF Roberts, EL Foesler, AG Salinger, Z Shaheen, X Shi, B Singh, J Tang, MA Taylor, PE Thornton, AK Turner, M Veneziani, H Wan, H Wang, S Wang, DN Williams, PJ Wolfram, PH Worley, S Xie, Y Yang, J-H Yoon, MD Zelinka, CS Zender, X Zeng, C Zhang, K Zhang, Y Zhang, X Zheng, T Zhou, and Q Zhu. 2019. "The DOE E3SM coupled model version 1: Overview and evaluation at standard resolution." *Journal of Advances in Modeling Earth Systems* 11(7): 2089–2129, https://doi.org/10.1029/2018MS001603

Gorelick, N, M Hancher, M Dixon, S Ilyushchenko, D Thau, and R Moore. 2017. "Google Earth Engine: Planetary-scale geospatial analysis for everyone." *Remote Sensing of Environment* 202: 18–27, https://doi.org/10.1016/j.rse.2017.06.031

Grimmond, CSB, M Blackett, MJ Best, J-J Baik, SE Belcher, J Beringer, SI Bohnenstengel, I Calmet, F Chen, A Coutts, A Dandou, K Fortuniak, ML Gouvea, R Hamdi, M Hendry, M Kanda, T Kawai, Y Kawamoto, H Kondo, ES Krayenhoff, S-H Lee, T Loridan, A Martilli, V Masson, S Miao, K Oleson, R Ooka, G Pigeon, A Porson, Y-H Ryu, F Salamanca, GJ Steeneveld, M Tombrou, JA Voogt, DT Young, and N Zhang. 2011. "Initial results from Phase 2 of the international urban energy balance model comparison." *International Journal of Climatology* 31(2): 244–272, https://doi.org/10.1002/joc.2227

Jackson, TL, JJ Feddema, KW Oleson, GB Bonan, and JT Bauer. 2010. "Parameterization of Urban Characteristics for Global Climate Modeling." *Annals of the Association of American Geographers* 100(4): 848–865, https://doi.org/10.1080/00045608.2010.497328

Krayenhoff, ES, T Jiang, A Christen, A Martilli, TR Oke, BN Bailey, N Nazarian, JA Voogt, MG Giometto, A Stastny, and BR Crawford. 2020. "A multi-layer urban canopy meteorological model with trees (BEP-Tree): Street tree impacts on pedestrian-level climate." *Urban Climate* 32: 100590, https://doi.org/10.1016/j.uclim.2020.100590

Krayenhoff, ES, AM Broadbent, L Zhao, M Georgescu, A Middel, JA Voogt, A Martilli, DJ Sailor, and E Erell. 2021. "Cooling hot cities: A systematic and critical review of the numerical modelling literature." *Environmental Research Letters* 16: 053007, https://doi.org/10.1088/1748-9326/abdcf1

Li, L, G Bisht, D Hao, and LR Leung. 2024. "Global 1 km land surface parameters for kilometer-scale Earth system modeling." *Earth System Science Data* 16(4): 2007–2032, https://doi.org/10.5194/essd-16-2007-2024

Li, X, Y Zhou, M Hejazi, M Wise, C Vernon, G Iyer, and W Chen. 2021. "Global urban growth between 1870 and 2100 from integrated high resolution mapped data and urban dynamic modeling." *Communications Earth & Environment* 2(1): 1–10, https://doi.org/10.1038/s43247-021-00273-w

Manoli, G, S Fatichi, M Schläpfer, K Yu, TW Crowther, N Meili, P Burlando, GG Katul, and E Bou-Zeid. 2019. "Magnitude of urban heat islands largely explained by climate and population." *Nature* 573(7772): 55–60, https://doi.org/10.1038/s41586-019-1512-9

Muller, CL, L Chapman, CSB Grimmond, DT Young, and X Cai. 2013. "Sensors and the city: A review of urban meteorological networks." *International Journal of Climatology* 33(7): 1585–1600, https://doi.org/10.1002/joc.3678

Oke, TR. 1979. Review of urban climatology, 1973-1976. Secretariat of the World Meteorological Organization Geneva.

Oleson, KW, GB Bonan, J Feddema, M Vertenstein, and E Kluzek. 2010. Technical description of an urban parameterization for the Community Land Model (CLMU). National Center for Atmospheric Research, Boulder, Colorado.

Paschalis, A, T Chakraborty, S Fatichi, N Meili, and G Manoli. 2021. "Urban Forests as Main Regulator of the Evaporative Cooling Effect in Cities." *AGU Advances* 2(2): e2020AV000303, https://doi.org/10.1029/2020AV000303

Qian, Y, T Chakraborty, J Li, D Li, C He, C Sarangi, F Chen, X Yang, and LR Leung. 2022. "Urbanization Impact on Regional Climate and Extreme Weather: Current Understanding, Uncertainties, and Future Research Directions." *Advances in Atmospheric Sciences* 39: 819–860, https://doi.org/10.1007/s00376-021-1371-9

Rothfusz, LP. 1990. The heat index equation (or, more than you ever wanted to know about heat index). National Oceanic and Atmospheric Administration, National Weather Service, Office of Meteorology, Fort Worth, Texas. SR 90-23.

Rubel, F, and M Kottek. 2010. "Observed and projected climate shifts 1901–2100 depicted by world maps of the Köppen-Geiger climate classification." *Meteorologische Zeitschrift* 19(2): 135–141, https://doi.org/10.1127/0941-2948/2010/0430

Sarangi, C, Y Qian, J Li, LR Leung, TC Chakroborty, and Y Liu. 2021. "Urbanization Amplifies Nighttime Heat Stress on Warmer Days over the US." *Geophysical Research Letters* 48(24): e2021GL095678, https://doi.org/10.1029/2021GL095678

Sharma, A, DJ Wuebbles, and R Kotamarthi. 2021. "The Need for Urban-Resolving Climate Modeling across Scales." *AGU Advances* 2(1): e2020AV000271, https://doi.org/10.1029/2020AV000271

Smith, A, N Lott, and R Vose. 2011. "The Integrated Surface Database: Recent Developments and Partnerships." *Bulletin of the American Meteorological Society* 92(6): 704–708, https://doi.org/10.1175/2011BAMS3015.1

Theeuwes, NE, JF Barlow, AJ Teuling, CSB Grimmond, and S Kotthaus. 2019. "Persistent cloud cover over mega-cities linked to surface heat release." *Npj Climate and Atmospheric Science* 2(1): 1–6, https://doi.org/10.1038/s41612-019-0072-x

Tuholske, C, K Caylor, C Funk, A Verdin, S Sweeney, K Grace, P Peterson, and T Evans. 2021. "Global urban population exposure to extreme heat." *Proceedings of the National Academy of Sciences of the United States of America* 118(41): e2024792118, https://doi.org/10.1073/pnas.2024792118

Wang, Z, J Song, PW Chan, and Y Li. 2021. "The urban moisture island phenomenon and its mechanisms in a high-rise high-density city." *International Journal of Climatology* 41(51): E150–E170, https://doi.org/10.1002/joc.6672

Yang, Q, X Huang, and Q Tang. 2019. "The footprint of urban heat island effect in 302 Chinese cities: Temporal trends and associated factors." *Science of the Total Environment* 655: 652–662, https://doi.org/10.1016/j.scitotenv.2018.11.171

Yang, Q, Y Xu, T Chakraborty, M Du, T Hu, L Zhang, Y Liu, R Yao, J Yang, S Chen, C Xiao, R Liu, M Zhang, and R Chen. 2024. "A global urban heat island intensity dataset: Generation, comparison, and analysis." *Remote Sensing of Environment* 312: 114343, https://doi.org/10.1016/j.rse.2024.114343

Zhang, T, Y Zhou, K Zhao, Z Zhu, G Chen, J Hu, and L Wang. 2022. "A global dataset of daily maximum and minimum near-surface air temperature at 1 km resolution over land (2003–2020)." *Earth System Science Data* 14(12): 5637–5649, https://doi.org/10.5194/essd-14-5637-2022

Zhao, L, X Lee, RB Smith, and K Oleson. 2014. "Strong contributions of local background climate to urban heat islands." *Nature* 511(7508): 216–219, https://doi.org/10.1038/nature13462

Zheng, Z, L Zhao, and KW Oleson. 2021. "Large model structural uncertainty in global projections of urban heat waves." *Nature Communications* 12(1): 1–9, https://doi.org/10.1038.s41467-021-24113-9

Ziter, CD, EJ Pedersen, CJ Kucharik, and MG Turner. 2019. "Scale-dependent interactions between tree canopy cover and impervious surfaces reduce daytime urban heat during summer." *Proceedings of the National Academy of Sciences of the United States of America* 116(15): 7575–7580, https://doi.org/10.1073/pnas.1817561116

U.S. DEPARTMENT OF
ENERGY

Office of Science